Heat and Mass Transfer Along a Wetted Porous Plate in an Air Stream

A. Belhamri
Institut National d'Enseignement Supérieur en Mécanique, Oum El Bouaghi, Algeria

J.-P. Fohr
Laboratoire d'Études Thermiques, 86022 Poitiers, France

This experimental study examines 2-D effects on long plate drying due to heat and moisture transfer through boundary layers and porous medium interaction. Many innovative techniques are used to measure accurately boundary layers (velocity, temperature, moisture), the wall surface (infrared sensors for temperature and moisture), and the medium (water content). Gradual decrease in surface saturation measured for several kinds of materials shows that their behavior is more complex than described by the Suzuki–Maeda model, which does not predict the mass exchange sufficiently. Based on the analysis of the transfer between the surrounding air and the porous medium at the scale of the pore on a rough surface, a flow classification is defined and other characteristics are proposed. The drying rate depends on the mass-transfer coefficient, which varies along the plate with the air flow. The study of boundary layers gives the corresponding profiles with an acceptable accuracy. The laminar-to-turbulent transition increases mass-transfer rates resulting in two drying fronts. The diffusive model proposed here predicts a gradual change in the drying rate along the plate similar to the experimental one.

Introduction

In convective industrial driers the products in question are generally stacked, allowing the free circulation of hot air (Rosen, 1987). In this kind of drying, the manufacturer has to regulate the air properties to limit the deformation of the material, such as warping, and to take into account the drying rate along the stack. The properties of exchange between the air and the material are determined from the internal state of the porous medium and the constitutive boundary layers around the pieces. In many driers, flat objects such as wood planks, tiles, clay, and plaster plates are laid along the flow and stacked on one or several levels. In this study, we will examine such a case of a porous plate along which an air stream is directed. The drying rate during the time is related to gradients across the plate (moisture, temperature, etc.) that depend on boundary layers (velocity, temperature, concentration) above the plate caused by viscosity effect and heat and mass-transfer diffusion.

Most of the drying studies, simulation models, or experimental drying rates are relative to one-dimensional transfer. The transfer coefficients at the plate surface are taken as constant. Some articles examine two-dimensional (2-D) plank drying induced by wood heterogeneity with constant transfer coefficients (Ouelhazi et al., 1992; Perré and Moyne, 1991) and less often a 2-D effect caused by variable transfer coefficients (Prat, 1991; Langrisch et al., 1992).

Many drying simulation models express all the physical properties of the medium: capillarity, vapor diffusion, adsorption, pressure effects, the simultaneous flowing of gas and liquid (Whitaker, 1980; Stanish et al., 1986; Ben Nasrallah and Perré, 1988; Ilic and Turner, 1989; Perré and Degiovanni, 1990). These models need some physical parameters, which are either difficult to obtain or acquired from questionable experiments. One can quote, for example, the relative permeabilities and the capillary pressure as functions of saturation (Daïan, 1992). These exhaustive simulation models are valuable tools for understanding this type of phenomenon, but they are too complex to optimize the performance of a drier. Other models, however, such as the diffusive ones (Crank, 1975; Toei, 1980), are more suitable for this purpose. All the simulations, obtained with constant

transfer coefficients at the external surface, show a strictly constant rate during the funicular capillary period, at which time the liquid flow rises to the free surface through a porous net. This is followed by a second period (the pendular period), which occurs after a sharp transition called the *critical point*. Some authors (Van Brakel, 1980; Kaviany and Mittal, 1987) suggest a transition period between the funicular period of constant drying rate (PCDR) and the pendular period of decreasing drying rate (PDDR), defined by a decreasing of the wet surface area. The surface state, not well known during the first period, determines the mass-transfer coefficients. It depends on the distribution of wet patches and boundary layers.

To better understand the surface phenomenon between these two characteristic periods, an experimental drying study on a porous plate in an environment of controlled air flow was carried out. In this investigation, we have used many innovative techniques to obtain very detailed measurements of the boundary layers, the porous medium, and most importantly the characteristics of the surface state. The chosen material as a representative of capillary-porous medium, nonhygroscopic or baraly, was a special light brick that offers a very good established PCDR.

Partially Wetted Surface Model

Suzuki – Maeda model

Suzuki–Maeda (S.M.) (1968) studied the mass transfer from an ideal smooth surface wetted in discontinuous periodic patches. The model consists of a 2-D diffusion equation in a boundary layer, which when fully developed leads to an analytic solution, assuming a linear velocity profile. The dimensionless number which governs the problem is $N = Dd/[\delta^2 u(\delta)]$, where $u(\delta)$ is the velocity at the distance δ of the wall, which is the thickness of the mass boundary layer.

The relative mass-transfer coefficient k/k_0 (k_0 for continuous wetting) is a function of this number N and the percentage of the wetted surface $\bar{\omega}$ (Figure 1). When $N \ll 1$ (or $d/\delta \ll 1$), the wet patch distribution has no influence at all on the mass transfer, nor does it have an influence on the drying rate.

Medium porosity and surface roughness

The S.M. model is simplified in regard to the real transfers between a porous medium and the surrounding boundary layers. The surface state of industrial materials that undergo drying are rarely smooth, and the surface roughness is a factor that produces an increase in the transfers. Industrial heat and mass exchangers are designed with regular turbulence promoters as ribs or steaks (fillets) (Krukreja et al., 1993), and for such cases the surface roughness can be defined by the geometry of these surface shapes. Materials for building, such as brick and perpend, do not offer similar obvious characteristics, and as a result some lengths have to be defined using statistical properties of the surface. The statistical analysis of the surface, that is, the roughness distribution, allows us to define a "representative surface cavity" of diameter α and deepness ϵ (Figure 2). For the glass beads frequently used in laboratories the roughness can be defined by a single parameter ($\alpha = \epsilon$) equal to the diameter of the mean bead.

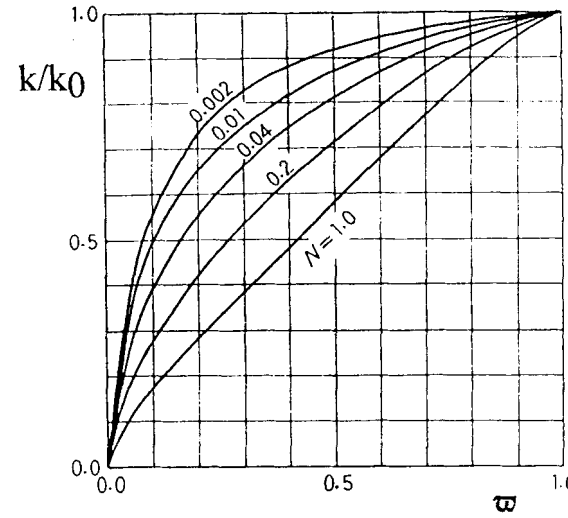

Figure 1. Suzuki–Maeda model.

Relative mass-transfer coefficient k/k_0 vs. percentage of wetted surface. $N = Dd/(d^2u(d))$, parameter.

The relation between the medium porosity and the surface roughness depends upon the manufacturing process. For example, ceramic burning creates glazed surfaces when the interior of the material remains porous. The porosity of a material is described by its pore distribution, measured with instruments such as a mercury porosimeter, from which we can define a representative diameter d or a range of diameters d_1, d_2 of pores. Finally, all of these lengths have to be compared with the thickness of the boundary layer in vapor concentration δ_c.

Dimensionless numbers that govern the mass transfer

Let us consider the general case of convective transfers above industrial capillary porous material with a rough surface. During the drying, at the end of the PCDR, the surface is not completely wetted and we have to consider a wet surface area decreasing when the capillary forces draw liquid toward the surface through the most narrow pores of the medium.

The mass transfer is determined from the boundary layers (velocity and vapor concentration), the pore distribution of the porous medium, and the state of the rough surface. We

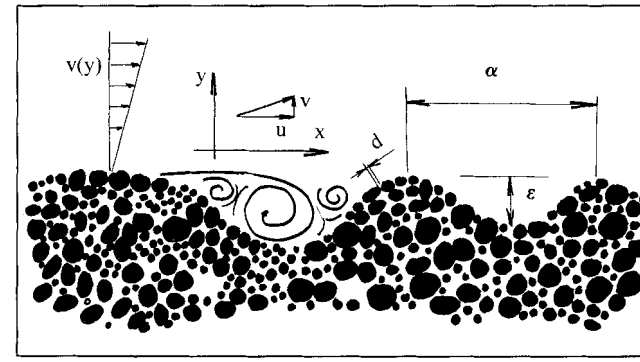

Figure 2. General surface state.

will now attempt to define mathematical criteria to classify these phenomena using transfer equations.

As local flow over a surface cavity can be three-dimensional and time-dependent, the constituent equations of conservation of mass, movement, and concentration are

$$\frac{\partial u}{\partial x}+\frac{\partial v}{\partial y}+\frac{\partial w}{\partial z}=0 \tag{1}$$

$$\rho\left(\frac{\partial u}{\partial t}+u\frac{\partial u}{\partial x}+v\frac{\partial u}{\partial y}+w\frac{\partial u}{\partial z}\right)=-\frac{\partial p}{\partial x}+\mu\left(\frac{\partial^2 u}{\partial x^2}+\frac{\partial^2 u}{\partial y^2}+\frac{\partial^2 u}{\partial z^2}\right) \tag{2}$$

$$\frac{\partial C}{\partial t}+u\frac{\partial C}{\partial x}+v\frac{\partial C}{\partial y}+w\frac{\partial C}{\partial z}=D\left(\frac{\partial^2 C}{\partial x^2}+\frac{\partial^2 C}{\partial y^2}+\frac{\partial^2 C}{\partial z^2}\right). \tag{3}$$

These equations can be the model of laminar or turbulent boundary layers, with appropriate coefficients μ and D, molecular or equivalent for the turbulence.

The scaling method (Bejan, 1984) consists of using reference parameters to compare the order of magnitude of each term in the equations. Following S.M., if we consider only the steady terms, the scales are $u(\delta_c)$, for u, δ_c for y, d pore or wet patch diameter for x, $C_{\text{ref}}=C(y=0)-C(y=\delta_c)$ for C.

Equation 1 leads to $(u/d)\sim(v/\delta_c)$ and Eq. 3 shows the order of the convective term (first member): $(u/d)C_{\text{ref}}$ and of the diffusive term (second member) $D(C_{\text{ref}}/\delta_c^2)$.

The ratio of the diffusive/convective fluxes leads to the first number of the problem:

$$N=\frac{Dd}{u(\delta_c)\delta_c^2}.$$

When the diffusive flux is negligible in relation to the convective flux ($N\ll 1$), the wet patch discontinuity has no influence on the mass transfer. According to experimental data, this number is stated as the ratio d/δ_c. Van Brakel (1980) uses X-rays to measure the moisture of a glass-bead layer, and shows that the water content of the surface decreases regularly during the first period of constant drying rate, but when $u(\delta_c)$ is fixed very high, δ_c decreases, and the drying rate becomes a sloped straight line.

The effect of the surface roughness must be examined at the scale of the microscopic cavities. The nature of the local flow is a function of a characteristic Reynolds number, Re. For example, following the wake evolution behind a cylinder, one can write:

- For $Re<1$, the streamlines of the laminar flow follow the surface geometry.
- For $Re>Re_{\text{cr}}$, the flow is established in a pseudoturbulent manner, and a turbulent diffusivity operates instead of the molecular diffusivity. Determination of the value of the critical number Re_{cr} needs special experimental studies (Puzach, 1992).
- For $1<Re<Re_{\text{cr}}$, the time-dependent eddy governs the transfer. A swirl sweeps the cavity and is periodically ejected into the boundary layer (Townes and Sabersky, 1966). This flow structure improves the mass transfer, and consequently a time-dependent convective transfer occurs instead of a steady diffusive one.

First we need to define a characteristic velocity for the cavity flow of depth $\epsilon\ll\delta_u$. The velocity of the sublayer can be expressed from the wall shear stress $\tau_w=\mu(\partial u/\partial y)_w$ as $u_{\text{ref}}=\tau_w(\epsilon/\mu)$. This velocity is linked to the shear flow velocity $u_*=\sqrt{\tau_w/\rho}$ as $u_{\text{ref}}=u_*^2(\rho\epsilon/\mu)$, thus $R_{\text{ref}}=(u_{\text{ref}}\epsilon/\nu)$, and $Re_{\text{ref}}=Re_*^2$, where Re_* or Re_{ref} is suitable for characterizing the air flow in the cavity.

Let us focus now on the time-dependent flow in the representative cavity defined by the two lengths, ϵ, α. When $1<Re_{\text{ref}}<Re_{\text{cr}}$, this flow inside the cavity is described by the Navier–Stokes equations, Eq. 2, where we assume that the inertial term is equivalent to the time-dependent term that is, $(\partial u/\partial t)\approx u(\partial u/\partial x)$. The scaling is written as $(\partial u/\partial t)\approx u_{\text{ref}}n$, and $u(\partial u/\partial x)\approx(u_{\text{ref}}^2/\alpha)$, which gives $u_{\text{ref}}=\alpha n$, where n is the order of the frequency of the swirl ejection.

Next, we have to compare the size of the cavity α with the representative pore diameter d. The ratio d/α should be a characteristic number of the problem. When α and d are of the same order of magnitude, which is generally the case for rough surfaces, the scale length in the flow direction x is α. If we compare the diffusive transfer $(D(\partial^2C/\partial x^2))$ to the convective time dependent one $(\partial C/\partial t)$, we obtain the number

$$N_*=\frac{D}{\alpha^2 n}.$$

Defining n and u_{ref}, this number becomes

$$N_*=\frac{\epsilon}{ScRe_*^2\,\alpha},$$

where Sc is the Schmidt number, ν/D. For $N_*\ll 1$ (large values of Re_*), the convective transfer in the cavity is predominant over the diffusive one. For $N_*\gg 1$ (small values of Re_*), the convective transfer in the cavity is negligible and the surface behaves as a perfectly smooth one.

It is obvious that the roughness increases the wall friction, but this does not always mean that the wall friction increases with the height (or diameter) of the rough elements. We must keep in mind that $\epsilon\ll\delta_c$, that is, the rough elements are present in the sublaminar layer. This property is illustrated in the article by Tao and Kaviany (1991). These authors studied mass transfer above a partially wetted surface composed of horizontal cylinders of diameter d that are not in contact. The thickness of concentration and velocity boundary layers have almost the same value. As expected, it is found (Figure 3) that the drying rate of the first period is greater when the velocity is high, but for fixed velocity and surface saturation, the drying rate decreases when the diameter of the cylinders increases. Moreover, in one case, this rate is greater with a reduced wet surface area than with a continuously smooth wetted one. These results can be interpreted with regard to the ratio of the cylinder diameter (d) to the mean boundary

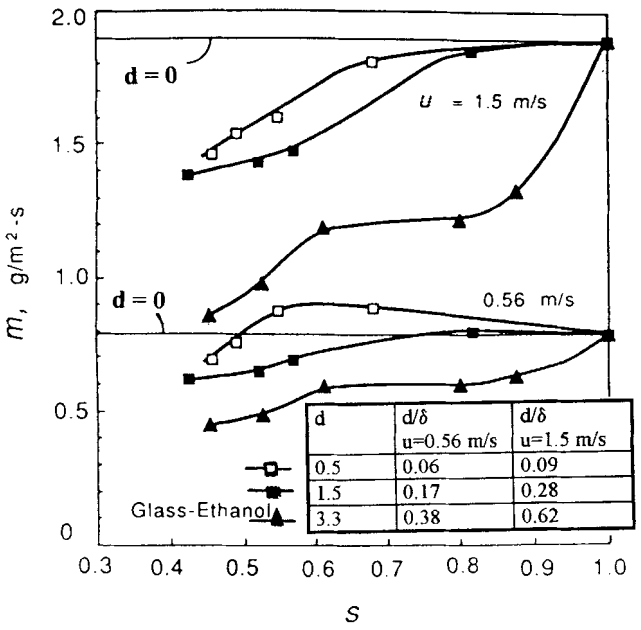

d	d/δ u=0.56 m/s	d/δ u=1.5 m/s
0.5	0.06	0.09
1.5	0.17	0.28
3.3	0.38	0.62

Figure 3. Drying rate from a two-dimensional partially covered liquid surface.

From Tao and Kaviany (1991). Abscissa S is a surface saturation; estimated δ (u_a = 1.5 m/s) = 0.53 cm and δ (u_a = 0.56 m/s) = 0.87 cm; $d = 0$ is the case of a perfectly flat and wet surface.

layer thickness (δ_c). The rapidly decreasing rate with surface saturation is obtained for $d/\delta_c \cong 0.6$ (the boundary layer thickness is estimated). The best rate improvement is obtained for $d/\delta_c \cong 0.06$. In the latter case, it is thought that the disturbance of the sublayer caused by the cylinders increases the wall friction and thus the mass transfer. When d/δ_c is high (≈ 1), the wall disturbance does not affect only the wall friction, but the entire boundary layer. For high values of this ratio, which are associated with the flow condition at $Re_{ref} < 1$, the streamlines follow a waving pattern along the surface.

We conclude in this section that the mass transfer above a rough surface of a porous material must be characterized with several numbers. For the more general case where the two lengths of the surface roughness α, ϵ are of the same order of magnitude, the transfer problem is explained using the following numbers:

$$N = \frac{Dd}{u(\delta_c)\delta_c^2}, \qquad Re_* = \frac{u_* \epsilon}{\nu}, \qquad \frac{d}{\alpha}.$$

The mass transfer increases when N decreases or Re_* increases. It can be assumed that the decreasing of the wet surface area does not affect the drying rate when N or $d/\delta c$ is low (S.M. model), or Re_* is high (turbulent diffusion or air sweeping in the cavities), or d/α is low.

Some experiments carried out on various materials, each of which has a particular behavior, confirm these propositions. The samples used for experiments, such as slabs of sintered bronze balls used for filtration, baked-earth pavement, or special light brick for pavement, come from the building materials industry.

Some special surfaces are excluded from this analysis. The dimensions of the surface cavities are in the range of $\alpha \ll \delta$ and $\alpha \approx \epsilon$. For deep cavities ($\epsilon \gg \alpha$), the transfer mechanism would be different. In the lower part of the cavity, the vapor diffusion remains the most important transfer force. For very large cavities ($\alpha \gg \epsilon$), the flow does not have the pattern of a swirl, and therefore the transfer properties are different (Perry et al., 1969).

Experimental Support and Metrology

The two parts of this study—the decreasing of the wet surface area and the drying development along the plate—are carried out using the same experimental setup. The plates of material that will undergo drying have been previously saturated with water in a vacuum chamber and laid on the axis of a wind tunnel where the velocity, temperature, and moisture of the air are regulated. The boundary layers defined by these three parameters expand from the round leading edge (Figure 4).

Boundary layer metrology

The velocity is obtained from the hot wire anemometry. The wire (5 μm diameter) is kept at a constant temperature and the calibration coefficients, which are dependent on the temperature, are taken from specific experiments. The temperature is obtained from the cold wire anemometry. The wire is subjected to a constant intensity and the electronic regulation corrects the velocity variations. A specific calibration is required. The moisture content is obtained from a capacitance-type instrument whose sensor is a thinly coated elementary area (1 cm × 1 cm; 0.3 mm thickness) directed in the air flow. The calibration is carried out in salt solution atmospheres. All the sensors are fixed on moving systems (1/50 mm accuracy).

Surface metrology

The surface temperature is obtained from an infrared radiation sensor (wavelength 8–14 μm). The emissivity factor of

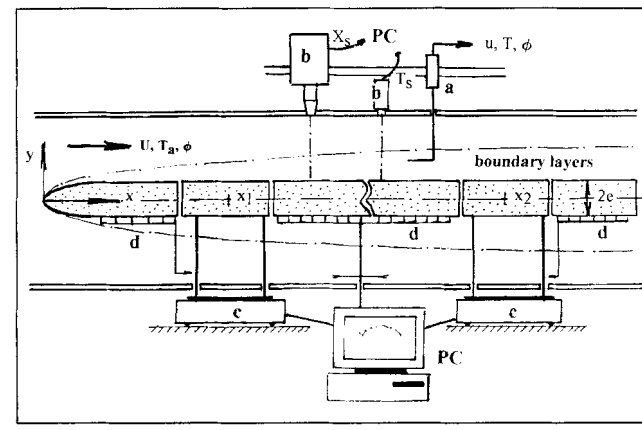

Figure 4. Area of measurement in the wind tunnel.

a, Boundary-layer metrology, hot and cold anemometry capacitance sensors; b, surface metrology, infrared temperature and moisture; c, weighing of samples; d, moisture of the brick plate; x_1 = 0.25 m, x_2 = 0.73 m.

the brick surface is deduced from comparison with a thermocouple on a specific experiment. The sensing head is fixed at the tunnel wall and receives the radiation through a hole. The area of measurement is about 2 cm in diameter. An electronic module delivers a linear output signal.

The surface moisture is obtained from a near-infrared photometric analyzer. The device compares the intensity of two reflected radiations, the first one (1.94 μm), as a reference, is slightly absorbed by water, and the second one, as a measure (1.80 μm), is widely absorbed. The output signal is a linear function of the surface moisture. The calibration requires two reference states, such as the dry state and the completely wet state. The interpretation of this type of measurement raises certain questions (Bowman et al., 1985). The emitted radiation is diffused mainly along the rough surface and secondarily through the pores of a thin surface layer. The area of measurement has a diameter of about 4 cm. The detector delivers an output signal linearized following the function $A + B \ln(Ir/Im)$, where I is the received radiation for the reference wavelength (r), and for the measure wavelength (m). This analytic form is founded on a simple reflective model and on some experimental calibrations (Schwartzberg, 1977).

When the area of measurement is moving on the surface plate, one observes important variations of the output signal, related to the surface heterogeneities of the medium. The reflected radiation varies with the structure of a surface layer of some wavelengths. For example, when one experiments with paper, it is shown that the acting layer consists of 2 or 3 sheets of paper. To avoid this difficulty, the signal is always relative to the same place and to a specific calibration defined by the saturation state. Following this method, the measurement can be reproduced and has an accuracy of 5%.

Drying rate

Two samples (10 cm large in the flow direction $\times$ 20 cm in the normal direction $\times$ 4 cm thickness) included in the drying floor (mean abscissas from leading edge $x_1 = 0.26$ m and $x_2 = 0.73$ m) can be continuously weighed on an electronic scale connected to the P.C. The drying rate is deduced from a statistical treatment of the data.

Moisture of the brick floor

The water content of the brick is obtained from resistivity measurements taken between needles stuck in the brick (1 cm deep, spaced every 1 to 4 cm). The resistivity between two needles is related to water content through a calibration carried out on samples kept at uniform moisture. The output signal is linear where $X < 20\%$ and depends on temperature. We consider that the measurement is rather that of the maximum than the mean moisture content in a 1-cm-thick layer under the surface. If we notice that the half-plate thickness is 2 cm (the drying is symmetrical above and below the floor), the measurement is a good approximation of the water content of the plate thickness.

Decrease of the Wet Surface Area

The simultaneous measurement of the drying rate, temperature, and moisture surface allows us to examine the decrease in the wet surface area and its influence on the mass-transfer coefficient. We examine this behavior during the drying of the three chosen materials.

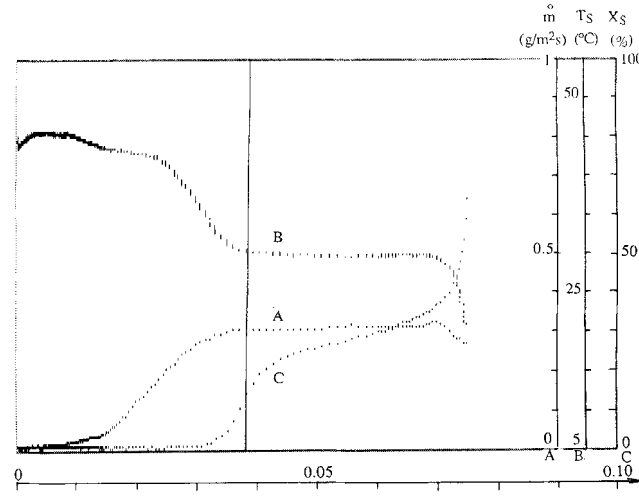

Figure 5. Drying of a sintered bronze balls plate.

$d = 600$ μm; $T_a = 50$°C; $\phi_a = 0.14$; $U = 2.1$ m/s; $e = 4.5$ mm; $x = x_1$; $\delta_u = 7$ mm; $\delta_c = 4$ mm. A, drying rate; B, surface temperature; C, moisture surface.

The slab of sintered bronze balls is an industrial material used for filtration, which has a simple geometry well known for capillary effects. The wetted sample is laid within the test board in the axis of the channel where it undergoes drying. We observe a continuous decrease in the wet surface area (Figures 5 and 6) during the first period where there is a constant drying rate. As predicted, the temperature does not vary from the wet bulb value. The period that shows a decrease in the drying rate begins when the surface moisture is very low. For this material, the characteristic numbers are the following: a small value of 7×10^{-4} for N ($d/\delta_c \cong 0.15$),

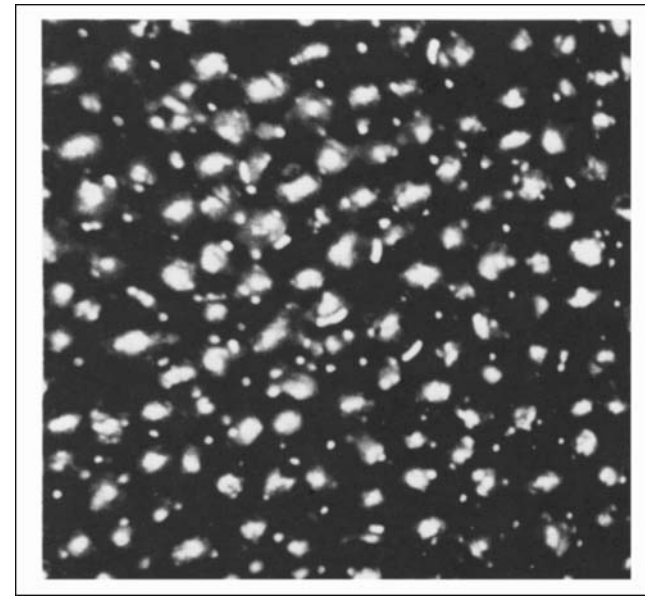

Figure 6. Drying of a sintered bronze balls plate.

Photography of the surface state. d balls = 600 μm; $\bar{X} = 6.2\%$; $X_{surf} = 19\%$ where the surface is close to the dry state.

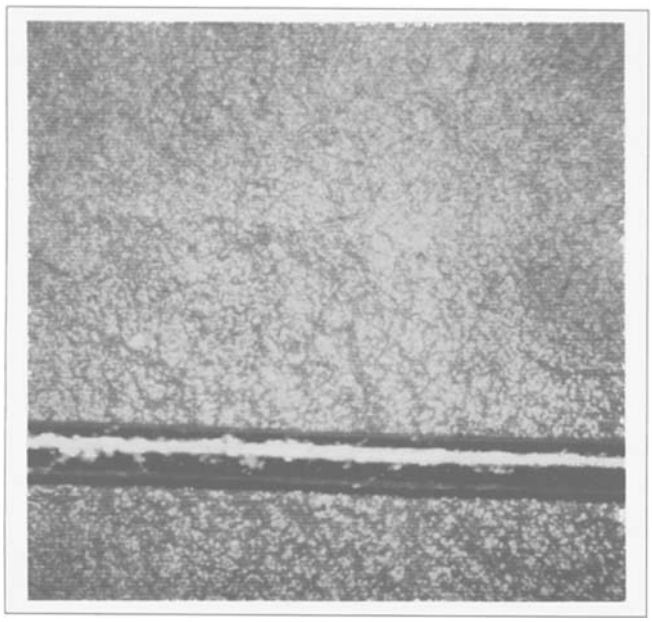

Figure 7. Drying of a baked-earth pavement plate.

Scale of photography: needle diameter 0.6 mm. The distribution of the wet patches is regular and gives an order of magnitude of the pore sizes.

but a high value of 4 for Re_*. The S.M. model cannot explain why the partially wetted surface has no effect on the drying rate. The influence of the roughness through Re_* is the key to the interpretation of the PCDR.

The second material is baked-earth pavement. The surface state is smooth and the pores are closely distributed around the 10-μm value (Figure 7). The drying results are similar to the previous ones, but we notice a significant difference when we compare the surface moisture curves (Figure 8). The surface moisture decreases continuously during the PCDR, and the PDDR begins when the surface moisture is high. The mean value d/δ_c along the sample is evaluated as 2.5×10^{-4}

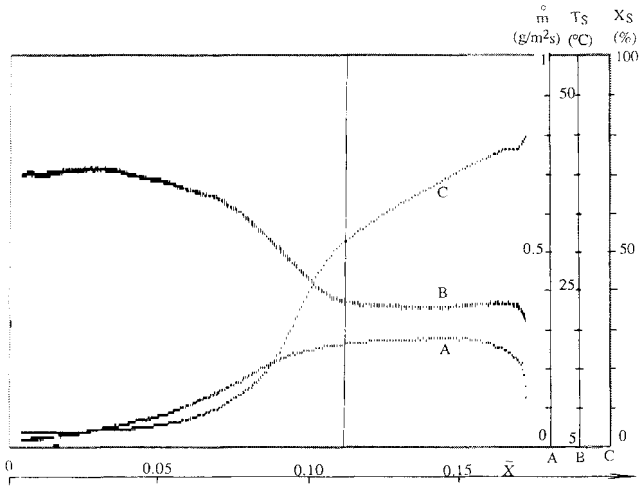

Figure 8. Drying of a baked-earth pavement plate.

$T_a = 50$°C; $\phi_a = 0.14$; $U = 4.6$ m/s; $e = 1.5$ cm; $d = 10$ μm; $x = x_1$; $\delta_u = 7$ mm; $\delta_c = 4$ mm. A, drying rate; B, surface temperature; C, surface moisture.

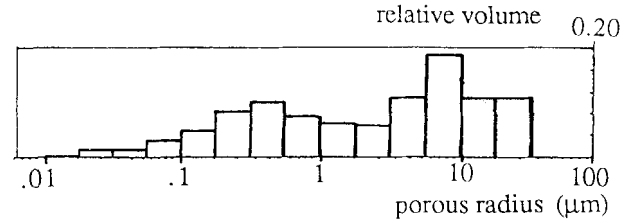

Figure 9. Pore distribution of the light brick obtained with a mercury porosimeter.

Weight of the sample: 0.4 g.

($N = 0.8\times10^{-5}$), which is more favorable for the transfer than the previous case. On the other hand, the roughness of the plate ($Re_* = 0.1$) is very low, which is less favorable than the previous case. Indeed the roughness scale of the bronze balls plate is of the order of the balls diameter (600 μm), whereas the roughness scale of the pavement is of the order of the pores diameter (about 10 μm). The surface roughness is an efficient means of increasing the wall velocity fluctuations (turbulence or intermittence) and thus the diffusion of moisture through the boundary layer.

The material used for the study of the gradual change along a plate is a very porous and special light brick (the complete saturation is about 40% d.b.). The pore distribution is large (Figure 9) and the surface state is very rough. The diameter of surface cavities is frequently about 1 mm (Figure 10). The cavities are distributed into the material but are not taken into account for the pore distribution. The latter is obtained with too small a sample (0.4 g) for a measurement of these macropores. The drying curves of this brick are very unusual (Figure 11). During the main part of the PCDR the surface moisture is constant. This surprising fact can be explained as follows: the internal macropores release water toward the surface through smaller pores that remain completely wet. It can be said that this material has a spongelike structure. The estimated value of N, calculated where $d_{\text{pore}} = 10$ μm, is low (1.4×10^{-5}) and the value of Re_*, calculated where $\alpha = 1$ mm, is 10. The roughness effect and the moisture distribution at the surface work together to produce a long period of constant drying rate.

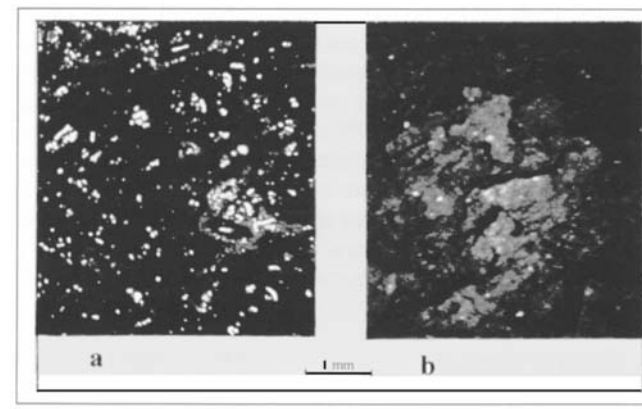

Figure 10. Surface state of the light brick.

$x = x_1$; $\delta_u = 4.4$ mm; $\delta_c = 2.6$ mm. (a) $\bar{X} = 35.5\%$; $X_{\text{surf}} = 100\%$. (b) $\bar{X} = 12\%$; $X_{\text{surf}} = 79.3\%$.

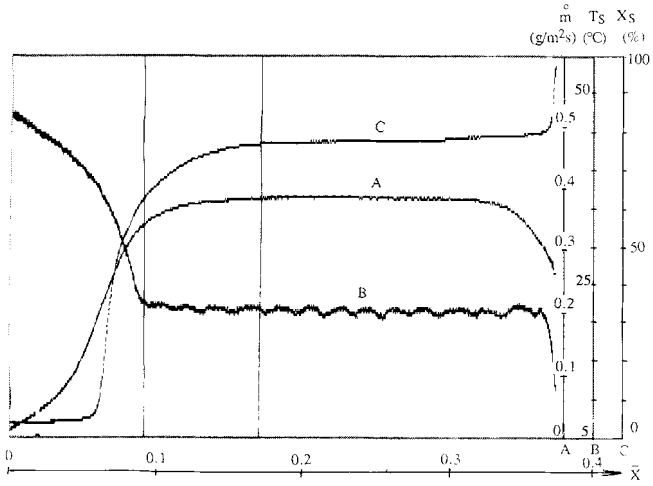

Figure 11. Drying of the light brick.

$T_a = 50°C$; $\phi = 0.14$; $U = 4.6$ m/s; $e = 3.7$ cm. A, drying rate; B, surface temperature; C, surface moisture.

Drying Development Along the Plate

Boundary layers

The investigation of the boundary layers (velocity, temperature, moisture), the surface state (temperature, moisture), and the plate water content allow us to follow the drying along the plate and determine the transfer coefficients. Figure 12 shows a typical profile along the plate. The gradual change along the wall of the velocity profile gives the wall friction through the momentum integral equation for 2-D incompressible boundary layers (Schlichting, 1968)

$$U^2\frac{d\theta}{dx} + (2\theta + \delta^*)U\frac{dU}{dx} = \frac{\tau_w}{\rho},$$

where

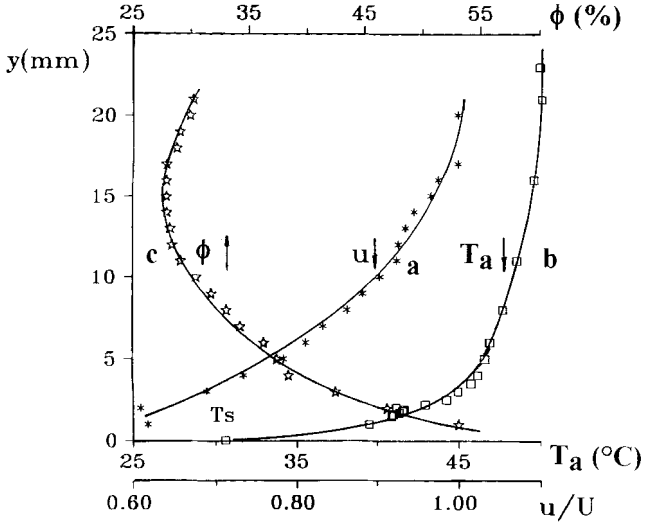

Figure 12. Boundary-layer profiles.

(a) Velocity; (b) temperature; (c) moisture; $U = 4.63$ m/s; $x = 0.73$ m; T_s—surface temperature obtained with infrared sensor.

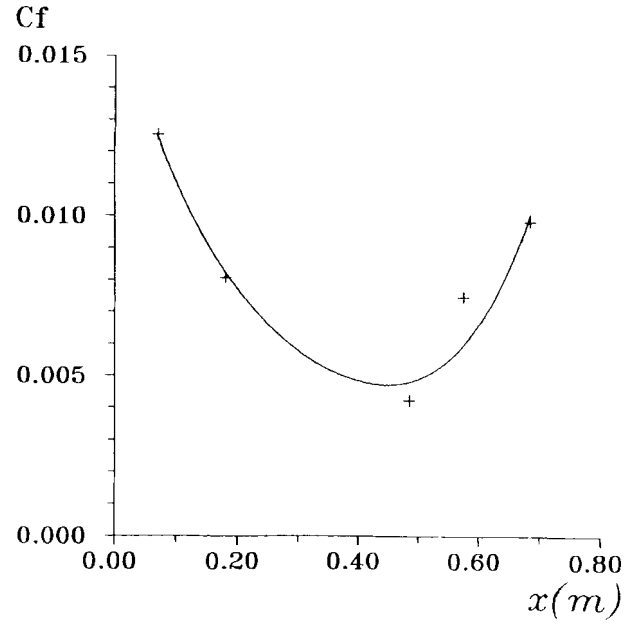

Figure 13. Variation of the wall friction coefficient along the plate.

$C_f = \tau_w/(0.5\rho U^2)$.

$$\theta = \int_0^\delta \frac{u}{U}\left(1 - \frac{u}{U}\right)dy, \qquad \delta^* = \int_0^\delta \left(1 - \frac{u}{U}\right)dy.$$

The gradual change of the wall friction coefficient $C_f = \tau_w/0.5\rho U^2$ (Figure 13) can be interpreted as a regular laminar decrease followed by an increase of the transition state toward the turbulence. The value of $C_f = 5 \cdot 10^{-3}$ is a common value for the beginning of the turbulence on a flat plate (Schlichting, 1968). The roughness of this material surface induces an early transition.

The transfer coefficients are determined when the whole part is in the PCDR. The heat transfer coefficient is obtained following three methods:

1. Analogy between the equation of boundary layer for the velocity and the temperature (Schlichting, 1968). We notice that during this period, these two layers begin at the same point. For the laminar part, the analogy is well known. Without specific data we use the correlation of the turbulent case for the transition part.

2. Derivation of the temperature profile associated with the infrared wall temperature:

$$h(T_a - T_w) = \lambda\left(\frac{\partial T}{\partial y}\right)_w.$$

3. Use of the drying rate. The heat used for evaporated water is supplied from the surrounding air:

$$h(T_a - T_w) = \Delta H_v.\dot{m}.$$

A correction for walls radiation is worked out. These three methods give reliable results (Figure 14), especially in the laminar part of the boundary layer.

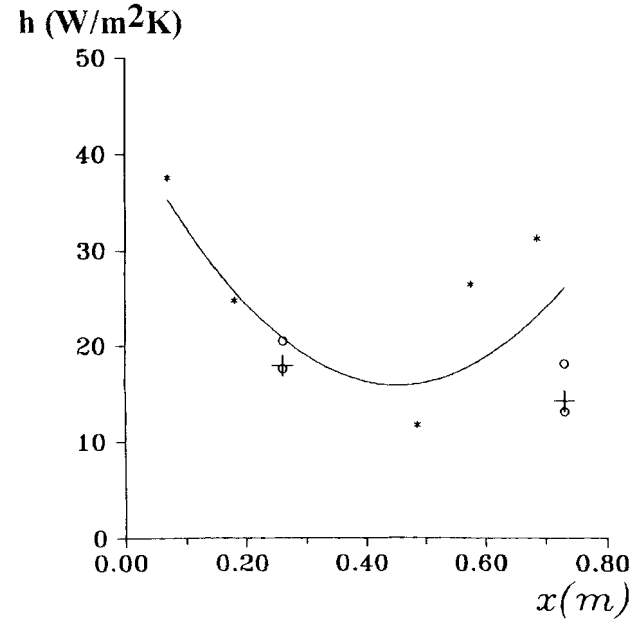

Figure 14. Variation of the heat-transfer coefficient along the plate.

*, Analogy with wall friction; +, from the drying kinetic; ○, from the temperature profile.

The mass-transfer coefficient can be obtained with the same methods (Figure 15). The Chilton–Colburn analogy gives:

$$k = \frac{h}{\rho C_p}\left(\frac{Pr}{Sc}\right)^{2/3}.$$

Methods (1) and (2) need highly accurate measurements. Indeed, the required measurement is not the volumetric mass ρ_v, but the relative moisture ϕ_a; the difference $\rho_{vs} - \rho_{va}$ is obtained from ϕ_a by

$$\rho_{vs} - \rho_{va} = \frac{p_{sv}(T_a)}{RT_a} M_v \left[\frac{p_{vs}(T_s)/T_s}{p_{vs}(T_a)/T_a} - \phi_a\right].$$

At the surface, we assume $\phi = 1$. If we consider the expression between brackets, a satisfactory measurement requires the accuracy of ϕ_a to be lower than 1% and that of T to be lower than 0.5°C. For example, where $x = 0.73$ m, the measurement are $T_a = 323$ K; $T_s = 303.5$ K; $\phi_a = 0.31$ and give:

$$\frac{p_{vs}(T_s)/T_s}{p_{vs}(T_a)/T_a} = 0.375.$$

For a T_s increase of 0.5°C, this ratio becomes 0.385. The limited accuracy is the moist air capacitance sensor ($\pm 1\%$).

Plate board

The surface temperature and moisture along the plate for successive drying time (Figures 16 and 17) correspond with the mass transfer coefficient. However, the surface temperature and moisture at the plate end remain very close to that of the leading edge. These curves show the gradual change from the first drying period to the second one. In most drying situations, the drying front moves in the flow direction. In this configuration, however, there are two fronts: the first one moves downstream from the leading edge and the second one moves upstream from the outlet edge.

The change in the water content in the plate during the second period of drying (Figure 18) corresponds with the latter result, but shows a more rapid drying rate in the first part of the plate. We must keep in mind that the measurement taken from the needles is that of a large part of the plate

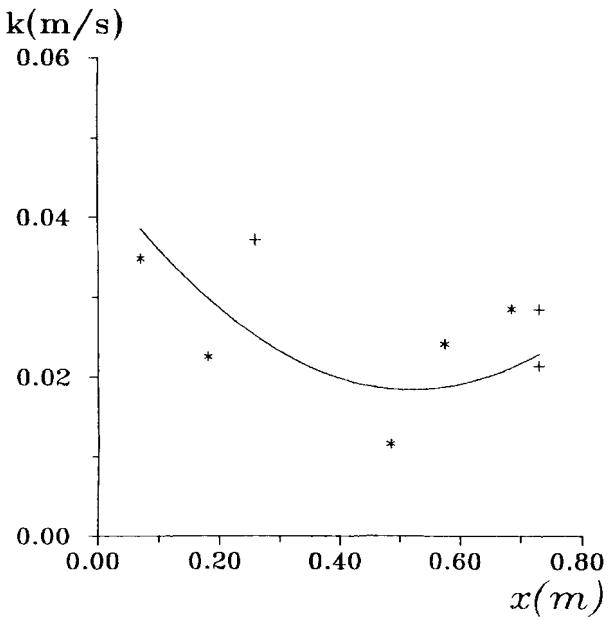

Figure 15. Variation of the mass-transfer coefficient along the plate.

*, Deduced from analogy with heat transfer; +, deduced from the drying kinetic.

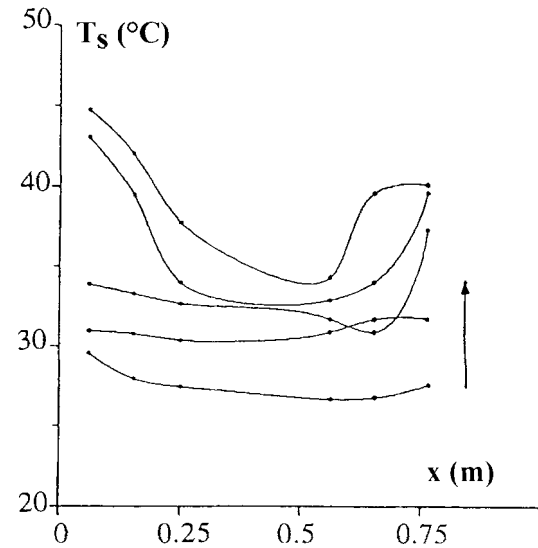

Figure 16. Surface temperature profile for successive drying times.

Successive drying time: 15, 16, 13.3, and 18.3 h. Read hours upward.

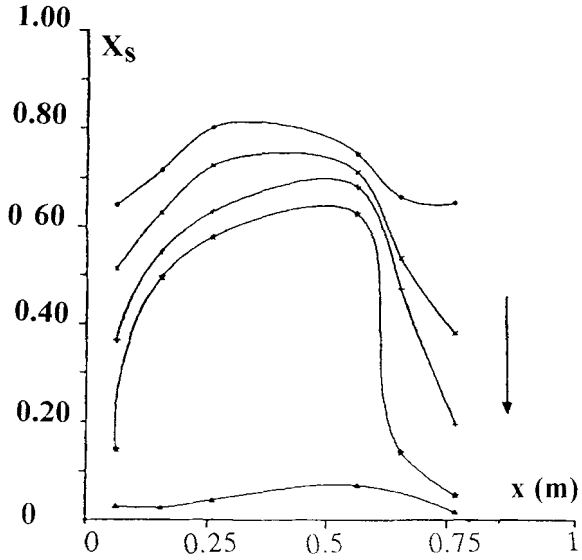

Figure 17. Surface moisture profile for successive drying times.

Successive drying time: 15, 16, 13.3, and 18.3 h. Read hours downward.

thickness, and above a 20% water content the measurement is not reliable. As soon as a part of the plate reaches the second drying period, the surface moisture is null and the transfer coefficients on this position and downstream are modified. Morever, the transition location of the boundary layer might move during the drying according to the evaporated mass flux.

Drying model

Only a drying model expressing moisture transfer into the plate and variations of transfer coefficients will permit the description of the drying as well as the optimization of the drier's performance. The diffusive model is suitable when the longitudinal transfers into the material are negligible relative to the transverse ones. The 1-D model is applied to a small length of the plate, for example, 1 cm, and a local exchange coefficient is applied. The model follows habitually diffusive problems (Crank, 1975), and takes into account these points:

- The experimental drying rates of the material are the only drying reference;
- The initial water content is uniform throughout the plate of $2e$ thickness $X(y,0) = X_i$;
- Two periods of drying are considered with two constant diffusion coefficients.

The PCDR is described by the system:

$$\frac{\partial X}{\partial t} = D_1 \frac{\partial^2 X}{\partial y^2}; \qquad t \in (0, t_{cr})$$

$$-\rho_s D_1 \left(\frac{\partial X}{\partial y}\right)_{y=-e,e} = F_0; \qquad \left(\frac{\partial X}{\partial y}\right)_{y=0} = 0$$

$$X(y,0) = X_i.$$

After some drying time, the series expressing the solution to this problem can be reduced, at which time a mean water content is obtained:

$$\bar{X} = \frac{1}{2e}\int_{-e}^{e} X dy \qquad \text{as} \qquad \bar{X} - X_i = -\frac{F_0 t}{r_s e},$$

where $F_0 = k(\rho_{vs}(T_s) - \rho_a)$; T_s is the wet bulb temperature; ρ_{vs} and ρ_a are function of T_a; and k is given in Figure 15.

At the end of the period, $X(y, t_{cr}) = X_0(y)$. The PDDR is described by the system:

$$\frac{\partial X}{\partial t} = D_2 \frac{\partial^2 X}{\partial y^2}; \qquad t \geq t_{cr}$$

$$X(\pm e, t) = X_{eq}; \qquad \left(\frac{\partial X}{\partial y}\right)_{y=0} = 0$$

$$X(y, t_{cr}) = X_0(y).$$

The solution $X(y,t)$ is expressed with a series, which can be reduced to the first term:

$$\bar{X} = A \sin\frac{\pi y}{2e} \exp\left(\frac{D_2 \pi^2 (t - t_{cr})}{4e^2}\right),$$

where

$$A = \frac{1}{e}\int_{-e}^{e} X_0(y) \sin\frac{\pi y}{2e} dy.$$

For this material X_{eq} is close to zero.

The diffusion coefficient D_2 is obtained from a regression using the experimental data $\bar{X}(t)$. This solution and the ex-

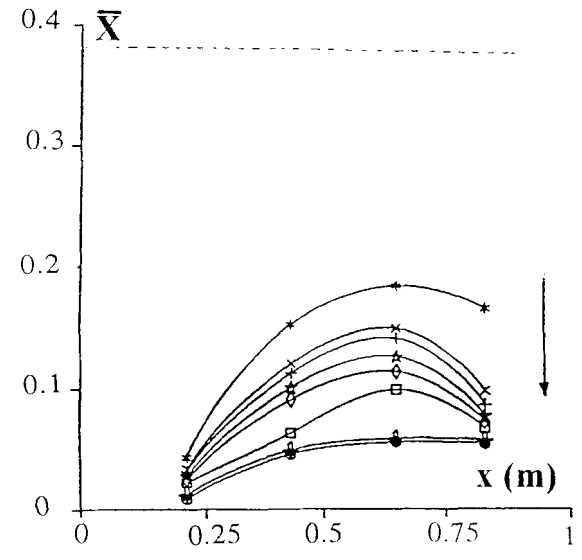

Figure 18. Water content profile of the brick plate during drying.

The measurement is not reliable above 20%. Successive time: 0 (horizontal line), 15, 16, 16.3, 16.6, 16.8, 17.2, 18.3, and 18.8 h.

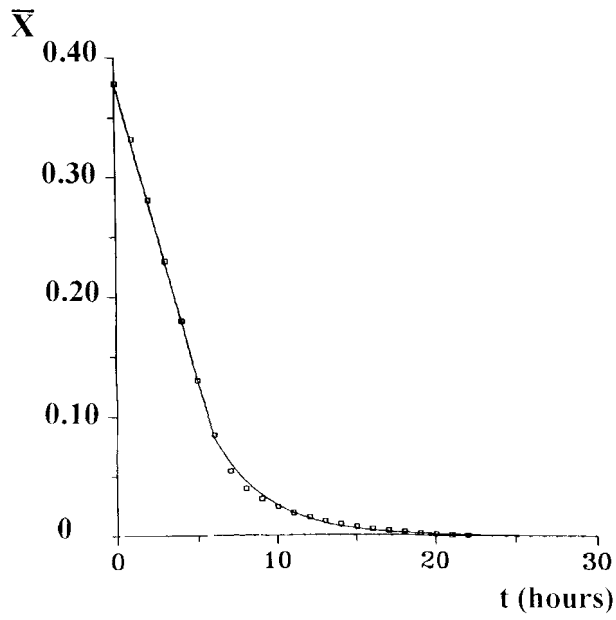

Figure 19. Adjustment of the diffusive model to the experimental drying rate.

$F_0 = 3.4 \times 10^{-4}$ kg/s·m^2.

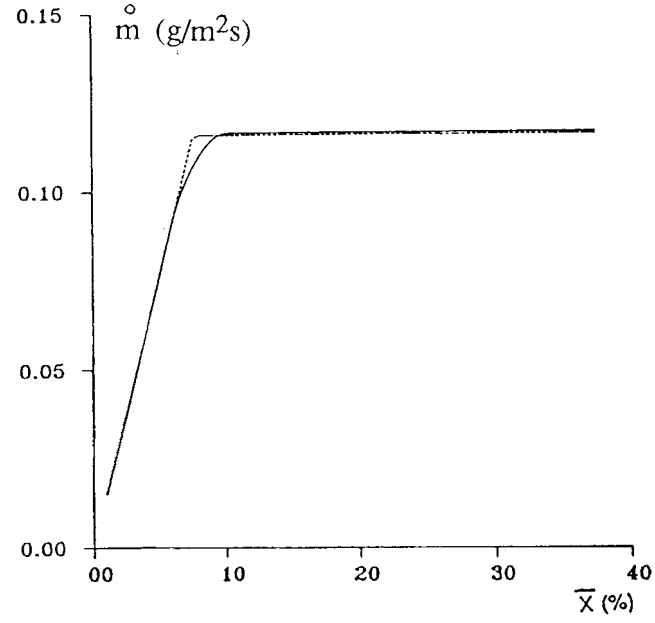

Figure 21. Simulated kinetic of sample whose length in the flow direction is fixed as: —— 10-cm-long sample; --- 1-cm-long sample.

perimental drying rate coincide (Figure 19). The accuracy of the drying simulation along the plate obtained with this model is linked to the accuracy of the mass exchange coefficient, especially when a part of the plate reaches the second drying period (PDDR). The two ends of the plate reach the PDDR while the central part remains at the PCDR. The concentration boundary layer decreases during drying, while the velocity boundary layer doesn't vary. If we consider that the concentration boundary layer begins at the point of abscissa x_0, the mass-transfer coefficient of a laminar boundary layer over the wet surface becomes (Bejan, 1984).

$$k_{cor}(x) = \frac{k(x)}{\sqrt{1-\left(\frac{x_0}{x}\right)^{0.75}}}.$$

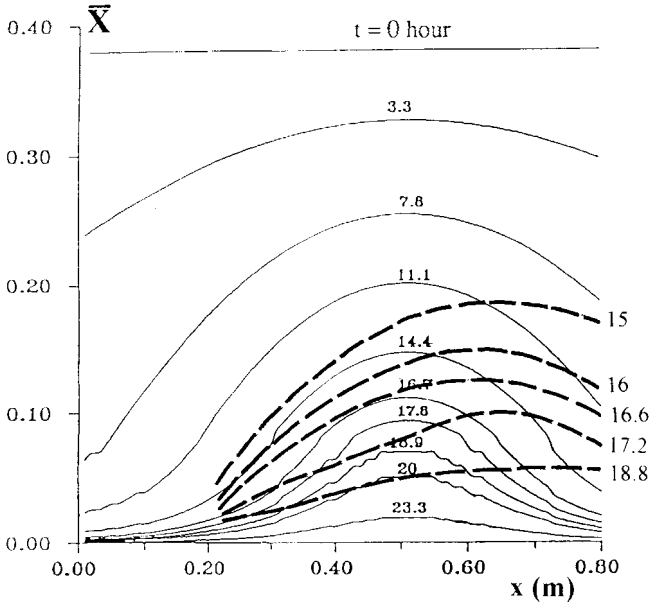

Figure 20. Water content profiles of the brick plate.

Diffusive model based on the experimental mass exchange coefficient. Comparison with experimental profiles (Figure 18). Successive time for the profiles of the diffusive mode are: 0 (horizontal line), 3.3, 7.8, 11.1, 14.4, 16.7, 17.8, 18.9, 20 and 23.3 h; for experiment profiles (dashed line): 15, 16, 16.6, 17.2, and 18.8 h. Read hours downward.

The simulated longitudinal profiles of the mean water content (Figure 20) can be compared to the experimental one. In this type of layer, reversing the flow does not seem adequate. The 2-D effect on the experimental drying rates can be evaluated from this simulation. The length of the sample, in the flow direction, is often about 10 cm. The drying rate measurement concerns a sample where one part can be in the PDDR and another part in the PCDR. The average measurement reduces the sharp transition on the drying curve between the first and the second period (Figure 21). One can make the following comments:

1. The experimental report should always specify the length of the sample used.
2. The observed transition between the two periods of the drying rate can be relative to two factors: the decrease in the wetted surface area and the sample length in the flow direction.

Conclusion

The drying behavior of a porous capillary medium is somewhat different when one considers a local section as compared to that of the entire plate laid in the drier. The fluid mechanics is the key to the gradual change of the transfer along the surfaces, and in this article we have pointed out that the transition from the laminar boundary layers toward

the turbulence is an important question. Prediction of the water content gradient along the plates depends on our knowing the location and the length of this transition. The position and development of this area depend on many factors: inlet turbulence intensity, inlet velocity direction, the shape of the leading edge, and wall roughness (Langrisch et al., 1992). The experimental correlations give mean values, which hide a notable discrepancy. The transition influence can lead to an intensity of drying during the first period as sizable in the outlet edge as in the inlet edge.

The direct and accurate measurement of mass-transfer coefficients is still a problem. The Colburn analogy between heat and mass transfer remains the most suitable way to obtain the mass-transfer coefficient during the PCDR. The influence of the gradual decrease of wet patches on mass transfer has to be considered by a more elaborate model than that of Suzuki–Maeda. It is not appropriate to adjust an equivalent mass-transfer coefficient with an experimental drying rate between the two drying periods. First, if the sample is too wide, the experimental data can be shifted around the critical point. Second, many factors must be identified at the source of the transfer: the origin of the velocity and mass boundary layers, the nature of the pores and the surface roughness with regard to the concentration boundary layer thickness, and finally a Reynolds number based on shear flow velocity.

The value of the mass-transfer coefficient can be questioned during the second period when a variable moisture condition prevails at the surface. Since the forces governing the transfer are situated in the porous medium during this period, a low value of accuracy for the transfer coefficient in the boundary layer does not disturb a reliable simulation.

Notation

C = concentration of water vapor in air
C_p = specific heat, $J \cdot kg^{-1} \cdot K^{-1}$
e = half thickness of the plate, m
F_0 = moisture rate, $kg \cdot m^{-2} \cdot s^{-1}$
h = heat-transfer coefficient, $W \cdot m^{-2} \cdot K^{-1}$
M = molar mass, kg
$\mathring{m}$ = drying rate, $kg \cdot m^{-2} \cdot s^{-1}$
p = pressure, Pa
R = ideal gas constant, 8.314 $J \cdot mol^{-1} \cdot K^{-1}$
t = time, s or h
u = horizontal component of velocity, $m \cdot s^{-1}$
U = velocity outside the boundary layer, $m \cdot s^{-1}$
v = vertical component of the velocity, $m \cdot s^{-1}$
w = third component of the velocity, $m \cdot s^{-1}$
x = coordinate along the horizontal plate, m
X = moisture content of the material (dry basis)
y = coordinate perpendicular to the plate, m

Greek letters

ΔH_v = latent heat of vaporization, $J \cdot kg^{-1}$
λ = conductivity, $W \cdot m^{-2} \cdot K^{-1}$
μ = dynamic viscosity, $kg \cdot m^{-1} \cdot s^{-1}$
ν = kinematic viscosity, $m^2 \cdot s^{-1}$

Subscripts

eq = equilibrium
i = initial
ref = reference
s = saturated
u = velocity
v = water vapor
$*$ = relative to the wall shear stress

Dimensionless numbers

$C_f = \tau_w/(0.5\rho U^2)$ wall friction coefficient
$N_* = \epsilon/(\alpha S_c R_{e*}^2)$
Pr = Prandtl number ($\mu C_p/\lambda$)

Literature Cited

Bejan, A., *Convection Heat Transfer*, Wiley, New York, p. 53 (1984).
Ben Nasrallah, S., and P. Perré, "Detailed Study of Model of Heat and Mass Transfer during Convective Drying for Porous Media," *Int. J. Heat Mass Transfer*, **31**(5), 957 (1988).
Bowman, G. E., A. W. Hooper, and L. Hantshorn, "A Prototype Infrared Reflectance Moisture Meter," *J. Agric. Eng. Res.*, **31**, 67 (1985).
Crank, J., *The Mathematics of Diffusion*, Clarendon Press, Oxford (1975).
Daïan, J. F., "From Pore Size Distribution to Moisture Transport Properties: Particular Problems for Large Pore Size Distributions," *Drying '92*, A. S. Mujumdar, ed., p. 263 (1992).
Ilic, M., and I. W. Turner, "Convective Drying of a Consolidated Slab of Wet Porous Material," *Int. J. Heat Mass Transfer*, **32**(12), 2351 (1989).
Kaviany, M., and M. Mittal, "Funicular State in Drying of a Porous Slab," *Int. J. Heat Mass Transfer*, **30**(7), 1407 (1987).
Krukreja, T. T., S. Lau, and R. D. McMillin, "Local Heat Mass Transfer Distribution in a Square Channel with Full and V-Shaped Ribs," *Int. J. Heat Mass Transfer*, **36**(8), 2013 (1993).
Langrisch, T. A. G., P. C. S. Kho, R. B. Keey, and J. C. F. Walker, "Experimental Measurement and Numerical Simulation of Local Mass Transfer Coefficients in Timber Kilns," *Drying Technol.*, **10**(3), 753 (1992).
Ouelhazi, N., G. Arnaud, and J. P. Fohr, "A Two-Dimensional Study of Wood Plant Drying. The Effect of Gaseous Pressure Below Boiling Point," *Transport Porous Media*, **7**, 39 (1992).
Perré, P., and C. Moyne, "Processes Related to Drying: Part II. Use of the Same Model to Solve Transfers both in Saturated and Unsaturated Porous Media," *Drying Technol.*, **9**(5), 1153 (1991).
Perré, P., and A. Degiovanni, "Simulation par volumes finis des transferts couplés en milieu poreux anisotropes: séchage du bois à basse et haute température," *Int. J. Heat Mass Transfer*, **33**(11), 2463 (1990).
Perry, A. E., W. H. Shofield, and P. N. Joubert, "Rough Wall Turbulent Boundary Layers," *J. Fluid Mech.*, **37**(2), 383 (1969).
Prat, M., "2D Modeling of Drying of Porous Media: Influence of Edge Effects at the Interface," *Drying Technol.*, **9**(5), 1181 (1991).
Puzach, V. G., "Heat and Mass Transfer on a Rough Surface with Gas Blowing at the Wall," *Int. J. Heat Mass Transfer*, **35**(4), 981 (1992).
Rosen, H. N., "Recent Advances in the Drying of Solid Wood," *Advances in Drying*, Vol. 4, Chap. 2, S. Mujumdar, ed. (1987).
Schlichting, H., *Boundary Layer Theory*, McGraw-Hill, New York, pp. 133, 268 (1968).
Schwartzberg, H. G., "Lightness and Darkness: The Reflectance of Dried Porous Foods," *AIChE Symp. Ser.*, Vol. 73, No. 163 (1977).
Stanish, M. A., G. S. Schager, and F. Kayihan, "A Mathematical Model of Drying for Hygroscopic Porous Media," *AIChE J.*, **32**(8), 1301 (1986).
Suzuki, M., and S. Maeda, "On the Mechanism of Drying of Granular Beds," *J. Chem. Eng. Japan*, **1**(1) (1968).
Tao, Y. X., and M. Kaviany, "Simultaneous Heat and Mass Transfer from a Two-Dimensional Partially Liquid-Covered Surface," *J. Heat Transfer, Trans. ASME*, **113**, 874 (1991).
Toeï, R., "Drying Mechanism of Capillary Porous Bodies," *Advances in Drying*, Vol. 2, Chap. 8, A. S. Mujumdar, ed. (1980).
Townes, H. W., and R. H. Sabersky, "Experiments on the Flow Over a Rough Surface," *Int. J. Heat Mass Transfer*, **9**, 729 (1966).
Van Brakel, J., "Mass Transfer in Convective Drying," *Advances in Drying*, Vol. 1, Chap. 7, A. S. Mujumdar, ed. (1980).
Whitaker, S., "Heat and Mass Transfer in Granular Porous Media," *Advances in Drying*, Vol. 1, Chap. 2, p. 146, A. S. Mujumdar, ed. (1980).

Manuscript received June 13, 1995, and revision received Sept. 25, 1995.